2017

Modelling and control of a novel walker robot for post-stroke gait rehabilitation

Emre Sariyildiz
University of Wollongong, emre@uow.edu.au

Hsiao-Ju Cheng
National Univeristy of Singapore

Gokhan M. Yagli
National Univeristy of Singapore

Haoyong Yu
National Univeristy of Singapore

Modelling and control of a novel walker robot for post-stroke gait rehabilitation

Abstract

In this paper, a novel walker robot is proposed for post-stroke gait rehabilitation. It consists of an omni-directional mobile platform which provides high mobility in horizontal motion, a linear motor that moves in vertical direction to support the body weight of a patient and a 6-axis force/torque sensor to measure interaction force/torque between the robot and patient. The proposed novel walker robot improves the mobility of pelvis so it can provide more natural gait patterns in rehabilitation. This paper analytically derives the kinematic and dynamic models of the novel walker robot. Simulation results are given to validate the proposed kinematic and dynamic models.

Keywords

modelling, control, rehabilitation, gait, post-stroke, robot, walker, novel

Disciplines

Engineering | Science and Technology Studies

Publication Details

Sariyildiz, E., Cheng, H., Yagli, G. M. & Yu, H. (2017). Modelling and control of a novel walker robot for post-stroke gait rehabilitation. IECON 2017 - 43rd Annual Conference of the IEEE Industrial Electronics Society (pp. 5221-5226). United States: IEEE.

Modelling and Control of a Novel Walker Robot for Post-Stroke Gait Rehabilitation

Emre Sariyildiz, *Member, IEEE*
School of Mechanical, Materials, Mechatronic and Biomedical Engineering, University of Wollongong, 2522, NSW, Australia.
emre@uow.edu.au

Hsiao-Ju Cheng, Gokhan Mert Yagli, Haoyong Yu
Department of Biomedical Engineering, National University of Singapore, Singapore.
hsiaojucheng@u.nus.edu, mert.yagli@u.nus.edu, bieyhy@nus.edu.sg

***Abstract*— In this paper, a novel walker robot is proposed for post-stroke gait rehabilitation. It consists of an omni-directional mobile platform which provides high mobility in horizontal motion, a linear motor that moves in vertical direction to support the body weight of a patient and a 6-axis force/torque sensor to measure interaction force/torque between the robot and patient. The proposed novel walker robot improves the mobility of pelvis so it can provide more natural gait patterns in rehabilitation. This paper analytically derives the kinematic and dynamic models of the novel walker robot. Simulation results are given to validate the proposed kinematic and dynamic models.**

Keywords—Human Robot Interaction; Kinematic and Dynamic Models; Stroke Rehabilitation; Walker Robot.

I. Introduction

Stroke is one of the leading causes of death overall the world [1]. According to a report from the American Heart Association, around 8 million population experience stroke onset every year worldwide [2]. It remains many sequalae including a pathological walking pattern. Impaired walking function refrains stroke survivors from not only activities of daily living but also social participation, which causes post-stroke depression in stroke survivors [3]. Unfortunately, the depressed mood also negatively influences on the recovery of daily functions [4–6]. Moreover, decreased mobility is associated with other diseases such as obesity which leads to comorbidity then raise the possibility to get recurrent strokes [7, 8]. This might become a vicious circle and form a huge economic burden for governments [9].

In the last decades, robot-assisted gait training has been proposed as a promising therapy for patients with stroke to regain their walking ability [10]. Some reviews and clinical trials have supported the positive effect of the robot-assisted gait training on the walking functions of patients with stroke. Build upon their findings, robot-assisted gait training could improve walking speed and quality of life [11–13]. However, most widespread commercial robots cannot satisfy the needs of different severity and stage of stroke survivors. For example, the Lokomat (Hocoma AG, Volketswil, Switzerland), one of the most popular robots for rehabilitation, is equipped with an overhead body weight support system and a lower limb exoskeleton. The latter constrains the lateral and rotational pelvic motions during walking [14]. Also, it has to be used with a treadmill so it cannot be used on over-ground training. Another example is Gait Trainer (Reha-Stim, Berlin, Germany). It is designed with two pedals as well as an overhead body weight support system [15]. Although it could lower the physical demands for clinicians, it was reported that there is no significant superiority over conventional therapy [16] and even efficacy as treadmill therapy [17].

In the light of the non-perfect rehabilitation robots for stroke survivors, our research team has developed a novel walker robot for them to regain their walking functions. This device consists of an omni-directional mobile platform, an active body weight support system, a force/torque sensor and an admittance control-based physical human-robot interaction interface. The pelvic motion of the patient is not constrained, and one can arbitrarily walk with protection and adequate body weight support. In addition, the walker robot can be applied over-ground so it provides more opportunities for users to explore the surrounding environment. It can deliver resistance training which is beneficial to strengthen muscles. Last but not least, the design of the walker robot is less bulky than Lokomat or Gait Trainer. In this paper, the kinematic and dynamic models of the novel walker robot are analytically derived. The models are very useful to design force/impedance controllers for gait training. The validity of the proposed models is verified by giving simulation results.

The rest of the paper is organized as follows. In section II, the novel walker robot is presented. In section III, kinematic and dynamic models of the walker robot are analytically derived. In section, IV, the models are verified by giving simulation results. The paper ends with conclusion given in section VI.

II. Novel Walker Robot

Fig. 1 illustrates the principle design concept and prototype of the novel walker robot.

The omni-directional walker robot, which is illustrated in Fig. 1a and Fig. 1b, is designed by using two active split offset castors. An active split offset castor, which is illustrated in Fig. 1c, is designed by using two conventional wheels. Thanks to the provided omni-directional motion of the walker robot, a patient can smoothly train lateral and rotational motions without consuming high energy.

In order to support body weight, a pelvic and trunk motion support brace unit is designed as shown in Fig. 1d. It is connected to a linear motor through a six-axis force/torque sensor which is shown in this figure. The linear motor is used to support the body weight of a patient during gait training. The horizontal and vertical interaction forces/torques are

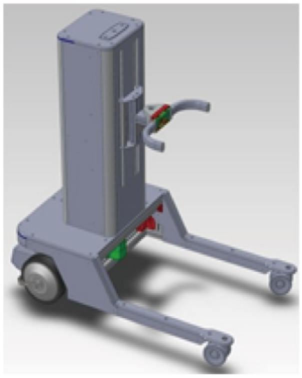

a) Principle of the walker robot.

b) Prototype of the walker robot.

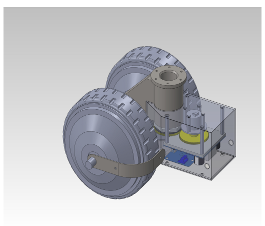

c) Active split offset castor.

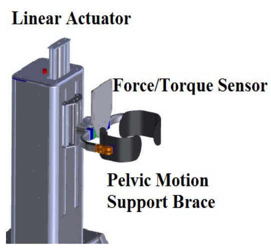

d) Body support brace unit.

Fig.1: The novel walker robot for post-stroke gait rehabilitation.

estimated by using the six-axis force/torque sensor. Different gait patterns can be generated for post-stroke rehabilitation by using the estimations of the interaction forces/torques.

The proposed walker robot is very useful for gait rehabilitation as it incorporates the trunk and pelvic movement which can induce a more natural gait pattern. It can assist in delivering over-ground gait training as well as lowering the physical burden of therapists per the body weight support system. In addition, the combination of body weight support and resistance training is promising to help the regain of muscle strength.

III. Kinematic and Dynamic Models of the Walker Robot

In this section, kinematic and dynamic models of the walker robot are analytically derived.

A. Kinematic Model of the Walker Robot

The kinematic model of the walker robot is illustrated in Fig.2. In this figure, the following apply:

$\{B\}$	World coordinate frame;
$\{C_i\}$	i^{th} active split offset castor's coordinate frame;
$\{P\}$	Omni-directional platform's coordinate frame;
α_{C_i}	Angle between $\{B\}$ and $\{C_i\}$;
ϕ	Angle between $\{B\}$ and $\{P\}$;
${}^{*}\mathbf{x}_{\bullet}$, ${}^{*}\mathbf{y}_{\bullet}$	Basis vectors of $\{\bullet\}$ w.r.t. $\{*\}$;
${}^{*}\mathbf{v}_{\bullet}$	Linear velocity vector of $\{\bullet\}$ w.r.t. $\{*\}$;
${}^{C_i}w_k$	Angular velocity of the i^{th} castor's k^{th} wheel;
${}^{B}\mathbf{p}_{B*}$	Distance between $\{B\}$ and $\{*\}$ w.r.t. $\{B\}$;

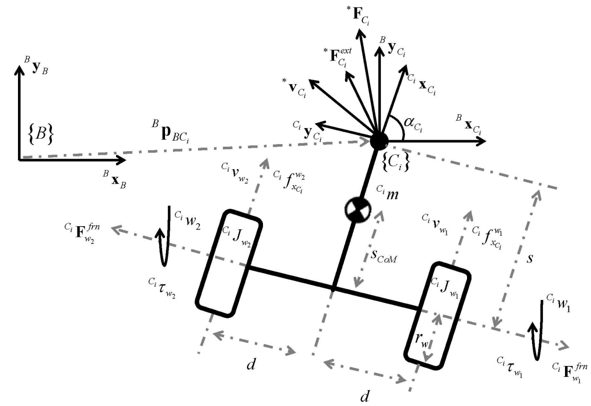

a) Active split offset castor.

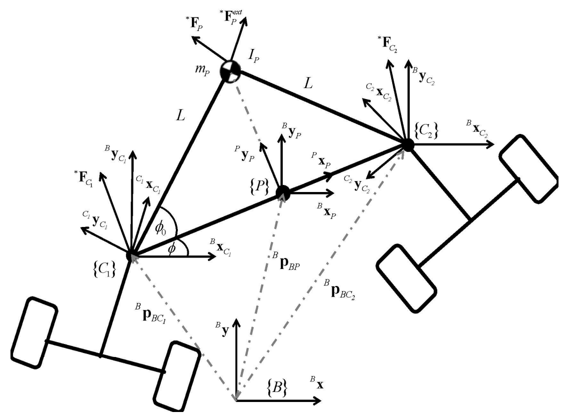

b) Omni-directional platform.

Fig.2: Kinematic and dynamic models of the novel walker robot.

r_w	Radius of the wheels;
d	Distance between wheel and support;
s	Distance between wheel and $\{C_i\}$;
L	Distance between the center of mass of the platform and $\{C_i\}$;
ϕ_0	Constant angle.

Velocity vector of the i^{th} active split offset castor can be derived in terms of its wheels' speeds by using

$$ {}^{B}\mathbf{v}_{C_i} = \mathbf{R}^{B}_{C_i}\mathbf{J}_{C_i}\,{}^{C_i}\mathbf{w} \tag{1}$$

where ${}^{B}\mathbf{v}_{C_i} = \left[{}^{B}\dot{x}_{C_i} \quad {}^{B}\dot{y}_{C_i}\right]^T$ represents velocity vector of the i^{th} castor w.r.t. $\{B\}$; ${}^{C_i}\mathbf{w} = \left[{}^{C_i}w_1 \quad {}^{C_i}w_2\right]^T$ represents angular velocity vector of the i^{th} castor's wheels; $\mathbf{J}_{C_i} = \frac{r_w}{2}\begin{bmatrix} 1 & 1 \\ s/d & -s/d \end{bmatrix}$ represents Jacobian matrix that relates wheels' speeds to the i^{th} castor's velocity vector which is described in $\{C_i\}$; and $\mathbf{R}^{B}_{C_i} = \begin{bmatrix} \cos(\alpha_{C_i}) & -\sin(\alpha_{C_i}) \\ \sin(\alpha_{C_i}) & \cos(\alpha_{C_i}) \end{bmatrix}$ represents rotation matrix between $\{B\}$ and $\{C_i\}$, such that

$$ \dot{\alpha}_{C_i} = \frac{r_w}{2d}\left({}^{C_i}w_1 - {}^{C_i}w_2\right) \tag{2}$$

where $\dot{\alpha}_{C_i}$ represents time derivative of α_{C_i}.

The velocity vector of the omni-directional platform can be similarly derived in terms of the active split offset castors' velocity vectors by using Eq. (1) and Fig. 2b as follows:

$$ {}^{B}\mathbf{v}_P = \mathbf{J}_P \, {}^{B}\mathbf{v}_C \tag{3} $$

where ${}^{B}\mathbf{v}_C = \begin{bmatrix} {}^{B}\mathbf{v}_{C_1} & {}^{B}\mathbf{v}_{C_2} \end{bmatrix}^T$ represents velocity vector of the active split offset castors w.r.t. $\{B\}$; ${}^{B}\mathbf{v}_P = \begin{bmatrix} {}^{B}\dot{x}_P & {}^{B}\dot{y}_P & \dot{\phi} \end{bmatrix}^T$ represents velocity vector of the omni-directional platform; and $\mathbf{J}_P = \frac{1}{2L\cos(\phi_0)} \begin{bmatrix} L\cos(\phi_0) & 0 & L\cos(\phi_0) & 0 \\ 0 & L\cos(\phi_0) & 0 & L\cos(\phi_0) \\ \sin(\phi) & -\cos(\phi) & -\sin(\phi) & \cos(\phi) \end{bmatrix}$ is the Jacobian matrix that relates the castors' velocity vectors to the omni-directional platform's velocity vector.

The forward kinematics of the walker robot is derived by combining Eq. (1) and Eq. (3) as follows:

$$ {}^{B}\mathbf{v}_P = \mathbf{J}_P \mathbf{R}_C^B \mathbf{J}_C \, {}^{C}\mathbf{w} \tag{4} $$

where $\mathbf{R}_C^B = \begin{bmatrix} \mathbf{R}_{C_1}^B & \mathbf{0}_{2\times2} \\ \mathbf{0}_{2\times2} & \mathbf{R}_{C_2}^B \end{bmatrix}$ and $\mathbf{J}_C = \begin{bmatrix} \mathbf{J}_{C_1} & \mathbf{0}_{2\times2} \\ \mathbf{0}_{2\times2} & \mathbf{J}_{C_2} \end{bmatrix}$ are rotation and Jacobian matrices, respectively; and ${}^{C}\mathbf{w} = \begin{bmatrix} {}^{C_1}\mathbf{w} & {}^{C_2}\mathbf{w} \end{bmatrix}^T$ is the angular velocity vector of the wheels.

Acceleration of the walker robot is derived by directly taking time derivative of Eq. (4) as follows:

$$ {}^{B}\dot{\mathbf{v}}_P = \dot{\mathbf{J}}_P \mathbf{R}_C^B \mathbf{J}_C \, {}^{C}\mathbf{w} + \mathbf{J}_P \dot{\mathbf{R}}_C^B \mathbf{J}_C \, {}^{C}\mathbf{w} + \mathbf{J}_P \mathbf{R}_C^B \mathbf{J}_C \, {}^{C}\dot{\mathbf{w}} \tag{5} $$

where $\dot{\mathbf{J}}_P = \frac{\dot{\phi}}{2L\cos(\phi_0)} \begin{bmatrix} 0 & 0 & 0 & 0 \\ 0 & 0 & 0 & 0 \\ \cos(\phi) & \sin(\phi) & -\cos(\phi) & -\sin(\phi) \end{bmatrix}$ represents time derivative of $\mathbf{J}_P$; $\dot{\mathbf{R}}_C^B = \begin{bmatrix} \dot{\mathbf{R}}_{C_1}^B & \mathbf{0}_{2\times2} \\ \mathbf{0}_{2\times2} & \dot{\mathbf{R}}_{C_2}^B \end{bmatrix}$ represents time derivative of $\mathbf{R}_C^B$ in which $\dot{\mathbf{R}}_{C_i}^B = \dot{\alpha}_{C_i} \begin{bmatrix} -\sin(\alpha_{C_i}) & -\cos(\alpha_{C_i}) \\ \cos(\alpha_{C_i}) & -\sin(\alpha_{C_i}) \end{bmatrix}$; ${}^{B}\dot{\mathbf{v}}_P = \begin{bmatrix} {}^{B}\ddot{x}_P & {}^{B}\ddot{y}_P & \ddot{\phi} \end{bmatrix}^T$ represents the acceleration vector of the platform; and ${}^{C}\dot{\mathbf{w}} = \begin{bmatrix} {}^{C_1}\dot{\mathbf{w}} & {}^{C_2}\dot{\mathbf{w}} \end{bmatrix}^T$ represents the angular acceleration vector of the castors' wheels in which ${}^{C_i}\dot{\mathbf{w}} = \begin{bmatrix} {}^{C_i}\dot{w}_1 & {}^{C_i}\dot{w}_2 \end{bmatrix}^T$.

Let us consider the following kinematic constraint of the omni-directional platform.

$$ {}^{B}\dot{x}_{C_1}\cos(\phi) + {}^{B}\dot{y}_{C_1}\sin(\phi) - {}^{B}\dot{x}_{C_2}\cos(\phi) - {}^{B}\dot{y}_{C_2}\sin(\phi) = 0 \tag{6} $$

where ${}^{B}\dot{x}_{\bullet}$ and ${}^{B}\dot{y}_{\bullet}$ represent time derivatives of ${}^{B}x_{\bullet}$ and ${}^{B}y_{\bullet}$, respectively.

The inverse of the Jacobian matrix $\mathbf{J}_P$ can be analytically derived by using Eq. (6) and Fig. 2b as follows:

$$ \mathbf{J}_P^{-1} = \begin{bmatrix} 1 & 0 & L\cos(\phi_0)\sin(\phi) \\ 0 & 1 & -L\cos(\phi_0)\cos(\phi) \\ 1 & 0 & -L\cos(\phi_0)\sin(\phi) \\ 0 & 1 & L\cos(\phi_0)\cos(\phi) \end{bmatrix} \tag{7} $$

Without suffering from singularity problem, the inverse kinematics of the walker robot can be analytically derived by using Eq. (4), Eq. (5) and Eq. (7) as follows:

$$ {}^{C}\mathbf{w} = \mathbf{J}_C^{-1} \mathbf{R}_B^C \mathbf{J}_P^{-1} \, {}^{B}\mathbf{v}_P \tag{8} $$

$$ {}^{C}\dot{\mathbf{w}} = \mathbf{J}_C^{-1} \dot{\mathbf{R}}_B^C \mathbf{J}_P^{-1} \, {}^{B}\mathbf{v}_P + \mathbf{J}_C^{-1} \mathbf{R}_B^C \dot{\mathbf{J}}_P^{-1} \, {}^{B}\mathbf{v}_P + \mathbf{J}_C^{-1} \mathbf{R}_B^C \mathbf{J}_P^{-1} \, {}^{B}\dot{\mathbf{v}}_P \tag{9} $$

where $\mathbf{R}_B^C = \left(\mathbf{R}_C^B\right)^{-1} = \begin{bmatrix} \mathbf{R}_B^{C_1} & \mathbf{0}_{2\times2} \\ \mathbf{0}_{2\times2} & \mathbf{R}_B^{C_2} \end{bmatrix}$ represents a rotation matrix in which $\mathbf{R}_B^{C_i} = \begin{bmatrix} \cos(\alpha_{C_i}) & \sin(\alpha_{C_i}) \\ -\sin(\alpha_{C_i}) & \cos(\alpha_{C_i}) \end{bmatrix}$; $\mathbf{J}_C^{-1} = \begin{bmatrix} \mathbf{J}_{C_1}^{-1} & \mathbf{0}_{2\times2} \\ \mathbf{0}_{2\times2} & \mathbf{J}_{C_2}^{-1} \end{bmatrix}$ represents inverse of the Jacobian matrix $\mathbf{J}_C$ in which $\mathbf{J}_{C_i}^{-1} = \frac{1}{r_w}\begin{bmatrix} 1 & d/s \\ 1 & -d/s \end{bmatrix}$; $\dot{\mathbf{R}}_B^C = \begin{bmatrix} \dot{\mathbf{R}}_B^{C_1} & \mathbf{0}_{2\times2} \\ \mathbf{0}_{2\times2} & \dot{\mathbf{R}}_B^{C_2} \end{bmatrix}$ represents time derivative of $\mathbf{R}_B^C$ in which $\dot{\mathbf{R}}_B^{C_i} = \dot{\alpha}_{C_i} \begin{bmatrix} -\sin(\alpha_{C_i}) & \cos(\alpha_{C_i}) \\ -\cos(\alpha_{C_i}) & -\sin(\alpha_{C_i}) \end{bmatrix}$; and $\dot{\mathbf{J}}_P^{-1} = \dot{\phi} \begin{bmatrix} 0 & 0 & L\cos(\phi_0)\cos(\phi) \\ 0 & 0 & L\cos(\phi_0)\sin(\phi) \\ 0 & 0 & -L\cos(\phi_0)\cos(\phi) \\ 0 & 0 & -L\cos(\phi_0)\sin(\phi) \end{bmatrix}$ represents time derivative of $\mathbf{J}_P^{-1}$.

B. Dynamic Model of the Walker Robot

Let us now derive the dynamic model of the walker robot by using Fig. 2. In this figure, the following apply:

s_{CoM}	Distance between support and center of mass;
${}^{C_i}\tau_{w_k}$	Motor torque of the ith castor's kth wheel;
${}^{C_i}f_{x_{C_i}}^{w_k}$	Applied force to the kth wheel of the ith castor in sagittal plane;
${}^{C_i}f_{y_{C_i}}^{w_k}$	Applied force to the kth wheel of the ith castor in frontal plane;
${}^{*}\mathbf{F}_{C_i}$	Force vector of the ith castor w.r.t. $\{*\}$;
${}^{*}\mathbf{F}_{C_i}^{ext}$	External force vector of the ith castor w.r.t. $\{*\}$;
${}^{*}\mathbf{F}_P$	Force vector of the platform w.r.t. $\{*\}$.
${}^{*}\mathbf{F}_P^{ext}$	External force vector of the platform w.r.t. $\{*\}$;
${}^{C_i}J_{w_k}$	Inertia of the ith castor's kth wheel;
m_{C_i}, I_{C_i}	Mass and inertia of the ith castor;
m_P, I_P	Mass and inertia of the platform.

Dynamic model of the ith active split offset castor's wheels is given in Eq. (10).

$$^{C_i}\mathbf{J}_w\,^{C_i}\dot{\mathbf{w}} = {}^{C_i}\boldsymbol{\tau}_w - {}^{C_i}\boldsymbol{\tau}_w^{dis} - r_w\,^{C_i}\mathbf{F}_w^{ext} \tag{10}$$

where $^{C_i}\mathbf{J}_w = \begin{bmatrix} ^{C_i}J_{w_1} & 0 \\ 0 & ^{C_i}J_{w_2} \end{bmatrix}$ represents inertia matrix of the ith castor's wheels; $^{C_i}\boldsymbol{\tau}_w = \begin{bmatrix} ^{C_i}\tau_{w_1} & ^{C_i}\tau_{w_2} \end{bmatrix}^T$ represents torque vector of the ith castor's wheels; $^{C_i}\boldsymbol{\tau}_w = \begin{bmatrix} ^{C_i}\tau_{w_1}^{dis} & ^{C_i}\tau_{w_2}^{dis} \end{bmatrix}^T$ represents disturbances at wheels, such as friction and backlash; and $^{C_i}\mathbf{F}_w^{ext} = \begin{bmatrix} ^{C_i}f_{w_1}^{ext} & ^{C_i}f_{w_2}^{ext} \end{bmatrix}^T$ represents external forces acting on the wheels of the ith castor's wheels.

Dynamic model of the ith active split offset castor can be directly derived from Fig. 2a as follows:

$$m_{C_i}\,^{C_i}\ddot{x}_{C_i} = {}^{C_i}f_{x_{C_i}} - {}^{C_i}f_{x_{C_i}}^{ext} \tag{11}$$

$$m_{C_i}\,^{C_i}\ddot{y}_{C_i} = {}^{C_i}f_{y_{C_i}} - {}^{C_i}f_{y_{C_i}}^{ext} \tag{12}$$

$$\mathrm{I}_{C_i}\ddot{\alpha}_{C_i} = \left({}^{C_i}f_{x_{C_i}}^{w_1} - {}^{C_i}f_{x_{C_i}}^{w_2}\right)d + \left({}^{C_i}f_{y_{C_i}}^{w_2} + {}^{C_i}f_{y_{C_i}}^{w_2}\right)s_{COG} - {}^{C_i}f_{y_{C_i}}^{ext}\left(s - s_{COG}\right) \tag{13}$$

where $^{C_i}f_{x_{C_i}} = {}^{C_i}f_{x_{C_i}}^{w_1} + {}^{C_i}f_{x_{C_i}}^{w_2}$ and $^{C_i}f_{y_{C_i}} = {}^{C_i}f_{y_{C_i}}^{w_1} + {}^{C_i}f_{y_{C_i}}^{w_2}$ represent sagittal and frontal forces of the ith castor in $\{C_i\}$, respectively; $^{C_i}f_{x_{C_i}}^{ext}$ and $^{C_i}f_{y_{C_i}}^{ext}$ represent sagittal and frontal external forces acting on the ith castor in $\{C_i\}$, respectively; and $\ddot{\alpha}_{C_i}$ represents angular acceleration of the ith castor, i.e., time derivative of $\dot{\alpha}_{C_i}$.

If $^{C_i}\dot{y}_{C_i} = s\dot{\alpha}_{C_i}$ and $^{C_i}\ddot{y}_{C_i} = s\ddot{\alpha}_{C_i}$ are substituted into Eq. (12) and Eq. (13), then

$$\frac{\mathrm{I}_{C_i} + m_{C_i}ss_{CoG}}{s}\,^{C_i}\ddot{y}_{C_i} = \left({}^{C_i}f_{x_{C_i}}^{w_1} - {}^{C_i}f_{x_{C_i}}^{w_2}\right)d - {}^{C_i}f_{y_{C_i}}^{ext}s \tag{14}$$

If $^{C_i}\dot{\mathbf{v}}_{C_i} = \begin{bmatrix} ^{C_i}\ddot{x}_{C_i} & ^{C_i}\ddot{y}_{C_i} \end{bmatrix}^T = \mathbf{J}_{C_i}\,^{C_i}\dot{\mathbf{w}}$ is substituted into Eq. (11) and Eq. (14), then the dynamic model is derived in matrix form as follows:

$$\mathbf{M}_{C_i}\,^{C_i}\dot{\mathbf{w}} = r_w\,^{C_i}\mathbf{F}_w - {}^{C_i}\mathbf{J}_{C_i}^T\,^{C_i}\mathbf{F}_{C_i}^{ext} \tag{15}$$

where $\mathbf{M}_{C_i} = \frac{r_w^2}{4}\begin{bmatrix} m_{C_i} + \frac{\mathrm{I}_{C_i} + m_{C_i}ss_{CoG}}{d^2} & m_{C_i} - \frac{\mathrm{I}_{C_i} + m_{C_i}ss_{CoG}}{d^2} \\ m_{C_i} - \frac{\mathrm{I}_{C_i} + m_{C_i}ss_{CoG}}{d^2} & m_{C_i} + \frac{\mathrm{I}_{C_i} + m_{C_i}ss_{CoG}}{d^2} \end{bmatrix}$ represents inertia matrix of the ith castor; $^{C_i}\mathbf{F}_w = \begin{bmatrix} ^{C_i}f_{x_{C_i}}^{w_1} & ^{C_i}f_{x_{C_i}}^{w_2} \end{bmatrix}^T$ represents tractive force vector of the ith castor's wheels; and $^{C_i}\mathbf{F}_{C_i}^{ext} = \begin{bmatrix} ^{C_i}f_{x_{C_i}}^{ext} & ^{C_i}f_{y_{C_i}}^{ext} \end{bmatrix}^T$ represents external forces acting on the ith castor in $\{C_i\}$.

Similarly, the dynamic model of the omni-directional platform can be directly derived from Fig. 2b as follows:

$$m_P\,^B\ddot{x}_P = {}^Bf_{x_p} - {}^Bf_{x_P}^{ext} \tag{16}$$

$$m_P\,^B\ddot{y}_P = {}^Bf_{y_p} - {}^Bf_{y_P}^{ext} \tag{17}$$

$$\tilde{\mathrm{I}}_P\ddot{\phi} = {}^B\tau_P - {}^B\tau_P^{ext} \tag{18}$$

where $^Bf_{x_p} = {}^Bf_{x_{C_1}} + {}^Bf_{x_{C2}}$ and $^Bf_{y_p} = {}^Bf_{y_{C_1}} + {}^Bf_{y_{C2}}$ represent horizontal forces of the omni-directional platform in $\{B\}$; $^B\tau_P = Lc_{\phi_0}s_\phi\,^Bf_{x_{C_1}} - Lc_{\phi_0}c_\phi\,^Bf_{y_{C_1}} - Lc_{\phi_0}s_\phi\,^Bf_{x_{C_2}} + Lc_{\phi_0}c_\phi\,^Bf_{y_{C_2}}$ represents vertical moment of the platform in which $c_\circ$ and $s_\circ$ represent $\cos(\circ)$ and $\sin(\circ)$, respectively; $^Bf_{x_P}^{ext}$, $^Bf_{y_P}^{ext}$ and $^B\tau_P^{ext}$ represent external forces and moment acting on the platform in $\{B\}$; $^B\ddot{x}_P$, $^B\ddot{y}_P$ and $\ddot{\phi}$ represent linear and angular accelerations of the platform in $\{B\}$; and $\tilde{\mathrm{I}}_P = \mathrm{I}_P + m_PL^2s_{\phi_0}^2$.

Equations (16-18) can be rewritten in matrix form by using

$$\mathbf{M}_P\,^B\dot{\mathbf{v}}_P = {}^B\mathbf{F}_P - {}^B\mathbf{F}_P^{ext} \tag{19}$$

where $\mathbf{M}_P = \begin{bmatrix} m_P & 0 & 0 \\ 0 & m_P & 0 \\ 0 & 0 & \tilde{\mathrm{I}}_P \end{bmatrix}$ represents inertia matrix of the platform; $^B\mathbf{F}_P = \begin{bmatrix} ^Bf_{x_P} & ^Bf_{y_P} & ^B\tau_P \end{bmatrix}^T$ represents force vector of the platform in $\{B\}$; and $^B\mathbf{F}_P^{ext} = \begin{bmatrix} ^Bf_{x_P}^{ext} & ^Bf_{x_P}^{ext} & ^B\tau_P^{ext} \end{bmatrix}^T$ represents external force vector of the platform in $\{B\}$.

Jacobian matrices satisfy the following force relations.

$$\begin{aligned} ^B\mathbf{F}_C &= \mathbf{J}_P^T\,^B\mathbf{F}_P \\ ^C\boldsymbol{\tau}_w &= \mathbf{J}_C^T\,^C\mathbf{F}_C \end{aligned} \tag{20}$$

where $^*\mathbf{F}_C = \begin{bmatrix} ^*\mathbf{F}_{C_1} & ^*\mathbf{F}_{C_2} \end{bmatrix}^T$ represents force vector of the castors w.r.t. $\{*\}$; and $^C\boldsymbol{\tau}_w = \begin{bmatrix} ^{C_1}\boldsymbol{\tau}_w & ^{C_2}\boldsymbol{\tau}_w \end{bmatrix}^T$ represents torque vector of the castors' wheels.

The dynamic models of the walker robot are derived by combining Eq. (10), Eq. (15) and Eq. (19) in joint and operational spaces as follows:

Joint Space:

$$^{JS}\mathbf{M}_{WR}\,^C\dot{\mathbf{w}} = {}^C\boldsymbol{\tau}_w - {}^C\boldsymbol{\tau}_w^{dis} - \mathbf{J}_{PC}^T\,^B\mathbf{F}_P^{ext} - \boldsymbol{\lambda}_{JS}\,^C\mathbf{w} \tag{21}$$

where $^{JS}\mathbf{M}_{WR} = {}^C\mathbf{J}_w + \mathbf{M}_C + \mathbf{J}_{PC}^T\mathbf{M}_P\mathbf{J}_{PC}$ represents the joint space inertia matrix of the walker robot in which $\mathbf{J}_{PC} = \mathbf{J}_P\,^B_C\mathbf{R}\,\mathbf{J}_C$ represents Jacobian matrix that relates the speed vector of the castors' wheels $^C\mathbf{w}$ to the velocity vector of the platform $^B\mathbf{v}_P$, $^C\mathbf{J}_w = \begin{bmatrix} ^{C_1}\mathbf{J}_w & \mathbf{0}_{2\times2} \\ \mathbf{0}_{2\times2} & ^{C_2}\mathbf{J}_w \end{bmatrix}$ represents inertia matrix of the castors' wheels and $\mathbf{M}_C = \begin{bmatrix} \mathbf{M}_{C_1} & \mathbf{0}_{2\times2} \\ \mathbf{0}_{2\times2} & \mathbf{M}_{C_2} \end{bmatrix}$

represents inertia matrix of the castors; ${}^{C}\boldsymbol{\tau}_w^{dis} = \left[{}^{C_1}\boldsymbol{\tau}_w^{dis} \quad {}^{C_2}\boldsymbol{\tau}_w^{dis} \right]^T$ represents disturbance vector of the castors' wheels; and $\boldsymbol{\lambda}_{JS} = \mathbf{J}_{PC}^T \mathbf{M}_P \left(\dot{\mathbf{J}}_P \mathbf{R}_C^B \mathbf{J}_C + \mathbf{J}_P \dot{\mathbf{R}}_C^B \mathbf{J}_C \right)$ represents nonlinear joint space Coriolis and centrifugal matrix.

Operational Space:

$$ {}^{OS}\mathbf{M}_{WR}\,{}^{B}\dot{\mathbf{v}}_P = \mathbf{J}_{CP}^T\,{}^{C}\boldsymbol{\tau}_w - \mathbf{J}_{CP}^T\,{}^{C}\boldsymbol{\tau}_w^{dis} - {}^{B}\mathbf{F}_P^{ext} - \boldsymbol{\lambda}_{OS}\,{}^{B}\mathbf{v}_P \tag{22} $$

where ${}^{OS}\mathbf{M}_{WR} = \mathbf{J}_{CP}^T \left({}^{C}\mathbf{J}_w + \mathbf{M}_C \right) \mathbf{J}_{CP} + \mathbf{M}_P$ represents the operational space inertia matrix of the walker robot in which $\mathbf{J}_{CP} = \mathbf{J}_C^{-1} \mathbf{R}_B^C \mathbf{J}_P^{-1}$ represents inverse of the Jacobian matrix $\mathbf{J}_{PC}$; and $\boldsymbol{\lambda}_{OS} = \mathbf{J}_{CP}^T \left({}^{C}\mathbf{J}_w + \mathbf{M}_C \right) \left(\mathbf{J}_C^{-1} \dot{\mathbf{R}}_B^C \mathbf{J}_P^{-1} + \mathbf{J}_C^{-1} \mathbf{R}_B^C \dot{\mathbf{J}}_P^{-1} \right)$ represents nonlinear operational space Coriolis and centrifugal matrix.

IV. Control of the Walker Robot

In this section, simulation results are given to verify the proposed kinematic and dynamic models of the walker robot which are derived in section III. In simulations, position and force trajectories of the omni-directional platform are controlled by designing position and force controllers in operational space. The simulation parameters are given in Table I.

To perform position control, a PD-type controller is designed in operational space by using

$$ {}^{B}\mathbf{F}_{WR}^{ref} = {}^{OS}\mathbf{M}_{WR} \left(K_D \left({}^{B}\mathbf{v}_P^{ref} - {}^{B}\mathbf{v}_P \right) + K_P \left({}^{B}\mathbf{x}_P^{ref} - {}^{B}\mathbf{x}_P \right) \right) + \boldsymbol{\lambda}_{OS}\,{}^{B}\mathbf{v}_P \tag{23} $$

where ${}^{B}\mathbf{F}_{WR}^{ref}$ represents the reference force of the walker robot in operational space when position control is performed.

To perform force control, a P-type controller is designed in operational space by using

$$ \mathbf{F}_{WR}^{ref} = {}^{OS}\mathbf{M}_{WR} K_F \left({}^{B}\mathbf{F}_P^{ref} - {}^{B}\mathbf{F}_P \right) + \boldsymbol{\lambda}_{OS}\,{}^{B}\mathbf{v}_P \tag{24} $$

where ${}^{B}\mathbf{F}_{WR}^{ref}$ represents the reference force of the walker robot in operational space when force control is performed.

The control signals of motors can be derived by using the following transformation between operational and joint spaces.

$$ {}^{C}\boldsymbol{\tau}_w^{ref} = \mathbf{J}_{PC}^T \mathbf{F}_{WR}^{ref} \tag{25} $$

Simulations are performed by neglecting internal and external disturbances such as parametric uncertainties due to inertia variations and nonlinear frictions and backlashes of actuators. However, it is impractical; i.e., disturbances should be considered to perform high-performance motion control applications in practice. For example, disturbance observer-based robust position and force controllers can be used to perform high-performance motion control applications by suppressing disturbances in practice [18-20].

Fig. 3 illustrates the simulation results of the position control; the linear motion is shown in Fig. 3a, and rotational motion is shown in Fig. 3b. As it is shown in this figure, the reference trajectories can be precisely tracked when the PD controller is implemented with the derived dynamic model.

Table I. Simulation parameters.

Parameter	Value	Description
r_w	101.60 mm	Radius of the wheels
d	71.5 mm	Distance between wheel and support
s	71.5 mm	Distance between wheel and $\{C_i\}$
L	800 mm	Distance between COM of platform and $\{C_i\}$
ϕ_0	0.523 rad.	Constant angle
m_P and I_P	45 kg and 2 kg m^2	Mass and inertia of the platform.
m_C and I_C	3 kg and 0.1 kg m^2	Mass and inertia of the castor.
${}^{C_i}J_{w_k}$	0.02 kg m^2	Inertia of wheel

In Fig. 4, Fig. 4a illustrates active force control result in which robot applies force to a moving environment, Fig. 4b illustrates passive force control result in which active environment applies external forces to the robot when it maintains zero interaction force, and Fig. 4c illustrates the position response of the robot in passive force control. Active and passive force control of the walker robot are very useful for gait rehabilitation. The former can be used to support patients in gait training or to strengthen the patients' muscles by applying forces in the reverse direction, and the latter provides high transparency in rehabilitation. As shown in Fig. 4b and Fig. 4c, the interaction force is minimized while the walker robot smoothly tracks its trajectory.

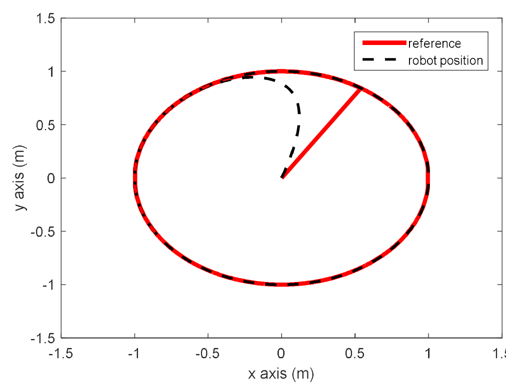

a) Linear position control in operational space.

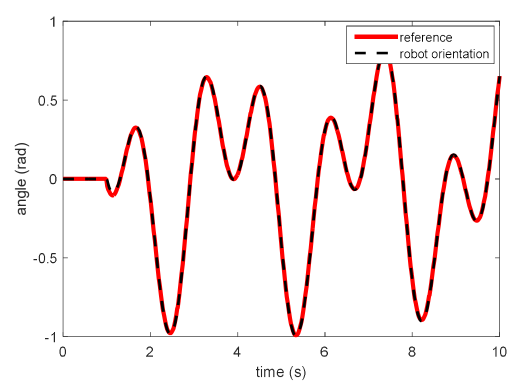

b) Orientation control in operational space.

Fig. 3: Position control results of walker robot.

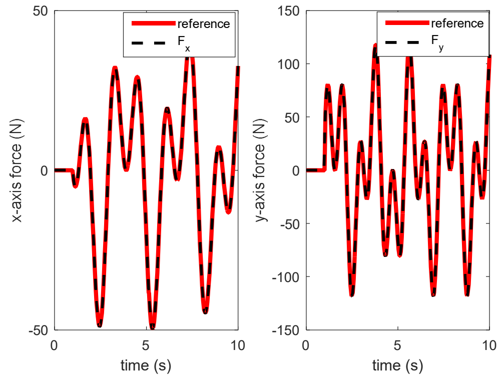

a) Active force control in operational space.

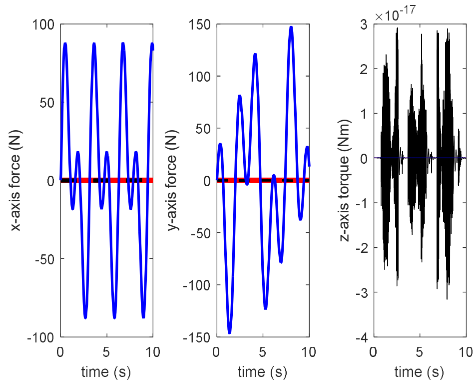

b) Passive force control in operational space. Blue curve is applied external force; red curve is zero force reference; and black curve is interaction force between robot and environment.

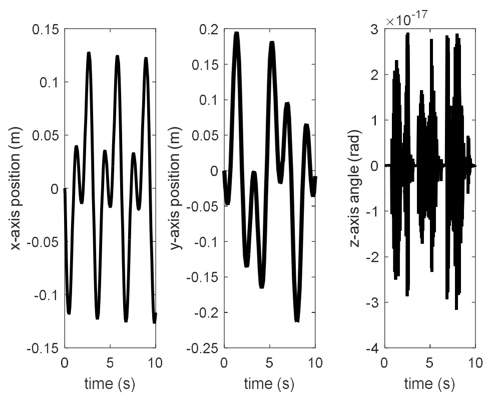

c) Position response of the walker robot in passive force control.

Fig. 4: Force control results of the walker robot.

V. Conclusion

This paper has proposed a novel walker robot for post-stroke gait rehabilitation. It can provide natural gait patterns thanks to the proposed omni-directional robotic platform. The kinematic and dynamic models of the walker robot are analytically derived and verified by giving position and force control simulation results. In the future, we plan to verify our models in the real system and design robust motion controllers to achieve high-performance in practice.

References

[1] WHO. Global status report on noncommunicable diseases 2014. http://www.who.int/nmh/publications/ncd-status-report-2014/en/. (accessed March 20, 2017)

[2] D. Mozaffarian, et al, "Executive Summary: Heart Disease and Stroke Statistics--2016 Update: A Report From the American Heart Association.," Circulation, vol. 133, no. 4, pp. 447–454, Jan. 2016.

[3] A. Srivastava, A. B. Taly, A. Gupta, and T. Murali, "Post-stroke depression: prevalence and relationship with disability in chronic stroke survivors.," Ann. Indian Acad. Neurol., vol. 13, no. 2, pp. 123–127, Apr. 2010.

[4] R. M. Parikh, R. G. Robinson, J. R. Lipsey, S. E. Starkstein, J. P. Fedoroff, and T. R. Price, "The impact of poststroke depression on recovery in activities of daily living over a 2-year follow-up.," Arch. Neurol., vol. 47, no. 7, pp. 785–789, Jul. 1990.

[5] F. B. van de Weg, D. J. Kuik, and G. J. Lankhorst, "Post-stroke depression and functional outcome: a cohort study investigating the influence of depression on functional recovery from stroke.," Clin. Rehabil., vol. 13, no. 3, pp. 268–272, Jun. 1999.

[6] E. Chemerinski, R. G. Robinson, and J. T. Kosier, "Improved recovery in activities of daily living associated with remission of poststroke depression.," Stroke., vol. 32, no. 1, pp. 113–117, Jan. 2001.

[7] G. E. Gresham, T. F. Phillips, P. A. Wolf, P. M. McNamara, W. B. Kannel, and T. R. Dawber, "Epidemiologic profile of long-term stroke disability: the Framingham study.," Arch. Phys. Med. Rehabil., vol. 60, no. 11, pp. 487–491, Nov. 1979.

[8] J. M. Guralnik, A. Z. LaCroix, R. D. Abbott, L. F. Berkman, S. Satterfield, D. A. Evans, and R. B. Wallace, "Maintaining mobility in late life. I. Demographic characteristics and chronic conditions.," Am. J. Epidemiol., vol. 137, no. 8, pp. 845–857, Apr. 1993.

[9] J. Persson, J. Ferraz-Nunes, and I. Karlberg, "Economic burden of stroke in a large county in Sweden.," BMC Health Serv. Res., vol. 12, p. 341, 2012.

[10] S. Fisher, L. Lucas, T. A. Thrasher, "Robot-assisted gait training for patients with hemiparesis due to stroke", Top Stroke Rehabil 18, pp. 269-276, 2011.

[11] R. Semprini, P. Sale, C. Foti, M. Fini, and M. Franceschini, "Gait impairment in neurological disorders: a new technological approach.," Funct. Neurol., vol. 24, no. 4, pp. 179–183, 2009.

[12] A. Pennycott, D. Wyss, H. Vallery, V. Klamroth-Marganska, and R. Riener, "Towards more effective robotic gait training for stroke rehabilitation: a review.," J. Neuroeng. Rehabil., vol. 9, p. 65, 2012.

[13] L. R. Sheffler and J. Chae, "Technological advances in interventions to enhance poststroke gait.," Phys. Med. Rehabil. Clin. N. Am., vol. 24, no. 2, pp. 305–323, May 2013.

[14] E. Swinnen, J. P. Baeyens, K. Knaepen, M. Michielsen, R. Clijsen, D. Beckwee, et al., "Robot-assisted walking with the Lokomat: The influence of different levels of guidance force on thorax and pelvis kinematics", Clin Biomech, 30, (3), pp. 254-9, 2015.

[15] S. Hesse, C. Werner, D. Uhlenbrock, S. von Frankenberg, A. Bardeleben, B. Brandl-Hesse, "An electromechanical gait trainer for restoration of gait in hemiparetic stroke patients: preliminary results", Neurorehabil Neural Repair, 15, (1), pp. 39-50, 2001.

[16] D. Dias, et al., "Can we improve gait skills in chronic hemiplegics? A randomised control trial with gait trainer.," Eura. Medicophys., vol. 43, no. 4, pp. 499–504, Dec. 2007.

[17] C. Werner, S. Von Frankenberg, T. Treig, M. Konrad, and S. Hesse, "Treadmill training with partial body weight support and an electromechanical gait trainer for restoration of gait in subacute stroke patients: a randomized crossover study.," Stroke., vol. 33, no. 12, pp. 2895–2901, Dec. 2002.

[18] E. Sariyildiz, and K. Ohnishi, "Robust Stability and Performance Analysis of the Control Systems with Higher Order Disturbance Observer: Frequency Approach", International Conference on Human System Interaction (HSI), Perth Australia, 6-8 June 2012.

[19] E. Sariyildiz, and K. Ohnishi, "Stability and Robustness of Disturbance Observer Based Motion Control Systems", IEEE Trans. on Ind. Electronics, Jan. 2015, vol. 62, no. 1, pp. 414-422.

[20] E. Sariyildiz, and K. Ohnishi, "An Adaptive Reaction Force Observer Design", IEEE Trans. on Mechatronics, Apr. 2015, vol. 20, no. 2, pp. 750-760.